REPORT No. 712

PROPELLER ANALYSIS FROM EXPERIMENTAL DATA

By GEORGE W. STICKLE and JOHN L. CRIGLER

SUMMARY

The operation of the propeller is analyzed by the use of the distribution of forces along the radius, combined with theoretical equations. The data were obtained in the NACA 20-foot wind tunnel on a 4-foot-diameter, two-blade propeller, operating in front of four body shapes, ranging from a small shaft to support the propeller to a conventional NACA cowling. A method of estimating the axial and the rotational energy in the wake as a fractional part of the propeller power is given. A knowledge of the total thrust and torque is necessary for the estimation.

The loss of efficiency due to the rotational velocity is always small for a propeller of optimum design, being only of the order of 1 percent for a low-solidity propeller. The loss of efficiency from this source may become quite large, however, at high blade-angle settings for a propeller with improper load distribution. Counterrotating propellers are shown to be attractive from considerations of aerodynamic efficiency only when propellers of high solidity are used. If high-solidity propellers are selected because of limitations on propeller diameter, it may be useful to resort to counterrotating propellers to eliminate the effect of the engine torque on the flying characteristics of the airplane, but only a small gain in propeller efficiency is normally to be expected.

The average angle of twist in the propeller slipstream is shown to be a function of the torque coefficient Q_c and charts are given to help estimate the angle. The increase in total pressure along the radius behind the propeller is given as a function of the power coefficient $1/\sqrt[5]{P_c}$ for use in estimating the available pressure that may be obtained for air intakes behind the propeller. The effect of the propeller-body shape upon the thrust and the torque distribution of the propeller is shown.

INTRODUCTION

The theoretical analysis of propeller operation has been investigated and the results of the investigation are summarized in reference 1. Many experimental studies of the operation of the entire propeller have also been made. In an attempt to combine the results of the investigations with those from theoretical analyses, it is necessary to know not only the total forces on the propeller but also the distribution of these forces along the radius. A method of obtaining the distribution of these forces from measurements in the wake of the propeller is given in reference 2.

In the present paper the distribution of thrust and torque along the radius is used to compare the actual performance of a propeller with the calculated performance. The energy losses in the wake of the propeller as obtained from experimental measurements are discussed. A method of determining these losses from the total thrust and torque of the complete propeller is given; the method permits an analysis of the effects of propeller solidity on the axial and the rotational losses of the propeller to be made from the total thrust and torque. The report presents data that show how and why the propeller efficiency is affected by the body shape. The data used in the analysis were obtained in the NACA 20-foot tunnel on a 4-foot-diameter, two-blade propeller operating in front of four body shapes, ranging from a small shaft to support the propeller to a conventional NACA cowling.

SYMBOLS

V velocity of air stream

u_0 velocity in plane of propeller (propeller removed)

ΔV velocity increase due to propeller

ρ mass density of air

q dynamic pressure of air stream ($1/2\rho V^2$)

n revolutions per second

D diameter of propeller

J advance-diameter ratio (V/nD)

P input power to propeller

Q input torque to propeller

T thrust of propeller (crankshaft tension)

u_0T useful work per unit time

C_P power coefficient ($P/\rho n^3D^5$)

C_Q torque coefficient ($Q/\rho n^2D^5$)

C_T thrust coefficient ($T/\rho n^2D^4$)

η true propeller efficiency

η_a apparent propeller efficiency $\left(\frac{TV}{P}=\frac{C_T}{C_P}\times\frac{V}{nD}\right)$

S disk area of propeller

T_c thrust disk-loading coefficient (T/qS)

P_c power disk-loading coefficient (P/qSV)

Q_c torque coefficient $(Q/\rho V^2D^3)$

$\frac{1}{\sqrt[3]{P_c}}=V\sqrt[5]{\frac{\rho S}{2P}}$

H_y differential pressure in yaw-head tubes due to twist of propeller slipstream

H_T total pressure behind propeller plane with propeller operating

H_{T_0} total pressure behind propeller plane with propeller removed

H increase in total pressure due to propeller $(H_T-H_{T_0})$

r radius to any blade element

R radius to tip of propeller

x $=r/R$

p geometric pitch

β propeller blade-angle setting at 0.75 R

K calibration constant for each yawmeter

$\frac{dC_T}{dx}$ differential thrust coefficient $(\pi Hx/2\rho n^2D^2)$

$\frac{dC_Q}{dx}$ differential torque coefficient $(\pi KH_yx^2/8\rho n^2D^2)$

a axial interference factor $\left(\frac{-1+\sqrt{1+4\frac{dC_T/dx}{\pi xJ^2}}}{2}\right)$

a' rotational interference factor $\left[\frac{dC_Q}{dx}\frac{2}{\pi^2Jx^3(1+a)}\right]$

E_a axial energy per unit time in slipstream

E_r rotational energy per unit time in slipstream

ψ angle of twist in the propeller slipstream

$$\left[\tan^{-1}\frac{4\frac{dQ_c}{dx}}{\pi(1+a)^2x^2}\right]$$

Ω angular velocity of propeller $(2\pi n)$

DERIVATION OF FORMULAS

The differential thrust and torque coefficients may be computed as follows (see reference 2):

$$\frac{dC_T}{dx}=\frac{\pi Hx}{2\rho n^2D^2} \quad (1)$$

$$\frac{dC_Q}{dx}=\frac{\pi KH_y^2x}{8\rho n^2D^2} \quad (2)$$

From the values of dC_T/dx, the axial interference factor a may be computed:

$$\frac{dC_T}{dx}=\pi xJ^2(1+a)a$$

$$a=\frac{-1+\sqrt{1+4\frac{dC_T/dx}{\pi xJ^2}}}{2} \quad (3)$$

From the values of dC_Q/dx and of a, the value of the rotational interference factor a' may be computed:

$$\frac{dC_Q}{dx}=\frac{\pi^2}{2}Jx^3(1+a)a'$$

$$a'=\frac{dC_Q}{dx}\frac{2}{\pi^2Jx^3(1+a)} \quad (4)$$

The values of the axial and the rotational interference factors obtained from these formulas are the average values. The flow at the propeller being continuous, this average value closely approximates the true value.

The amount of total pressure added by the propeller to the slipstream in terms of the dynamic pressure of the air stream may be obtained directly from equation (1)

$$H=\frac{2\rho n^2D^2}{\pi x}\frac{dC_T}{dx}$$

$$\frac{H}{q}=\frac{4\frac{dC_T}{dx}}{\pi J^2x} \quad (5)$$

From the force measurements, the value of the apparent propeller efficiency is

$$\eta_a=\frac{TV}{P} \quad (6)$$

If the velocity in the propeller plane with the propeller removed u_0 is equal to V at all radii, then the value of η_a obtained by means of equation (6) is the true propeller efficiency. If u_0 is different from V, the true propeller efficiency may be computed from η_a by the use of the curves of the thrust distribution and the velocity distribution with the propeller removed, according to the following relation:

$$\eta=\eta_a\frac{\int_0^1\frac{u_0}{V}\frac{dC_T}{dx}dx}{\int_0^1\frac{dC_T}{dx}dx} \quad (7)$$

The energy imparted to the propeller slipstream per unit time may be computed from the curves of thrust and torque distribution and the interference velocities. The energy lost per unit time in axial velocity may be written

$$E_a=\int aVdT=\rho n^2D^4V\int_0^1 a\frac{dC}{dx}dx \quad (8)$$

If E_a is divided by the power input to the propeller, the fractional part of power lost in axial energy is obtained:

$$\frac{E_a}{P}=\frac{\rho n^2D^4V}{P}\int_0^1 a\frac{dC_T}{dx}dx=\frac{J}{C_P}\int_0^1 a\frac{dC_T}{dx}dx \quad (9)$$

The energy lost per unit time in rotational velocity may be written

$$E_r=\int a'\Omega dQ=2\pi\rho n^3D^5\int_0^1 a'\frac{dC_Q}{dx}dx \tag{10}$$

The fractional part of the power lost in rotational energy may then be written

$$\frac{E_r}{P}=\frac{2\pi\rho n^3D^5}{P}\int_0^1 a'\frac{dC_Q}{dx}dx$$

$$=\frac{2\pi}{C_P}\int_0^1 a'\frac{dC_Q}{dx}dx \tag{11}$$

$$=\frac{1}{Q_c}\int_0^1 a'\frac{dQ_c}{dx}dx \tag{11a}$$

The fractional part of the power unaccounted for from the foregoing analysis may be computed as follows:

$$\text{Remainder } \frac{E}{P}=1-\left(\eta+\frac{E_a}{P}+\frac{E_r}{P}\right) \tag{12}$$

This remainder of the power consists of the errors in calculation of energy in axial and rotational velocities caused by the nonuniform character of the wake and of the energy represented in the profile drag of the blades, which is in the form of random velocities and of heat.

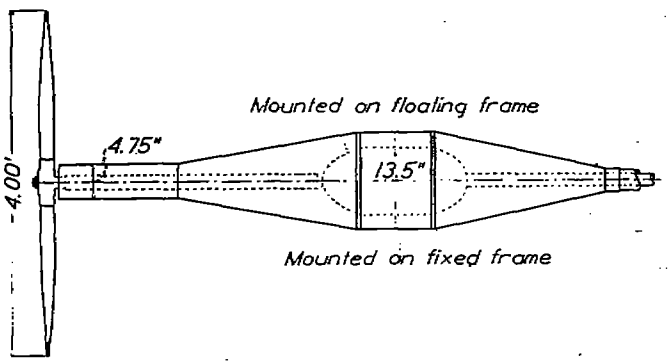

FIGURE 1.—Test arrangement of free-air body.

The angle of twist in the propeller slipstream immediately behind the propeller may be computed from the axial and the angular velocities:

$$\tan\psi=\frac{2\pi rn(2a')}{V(1+a)}=\frac{2\pi xa'}{J(1+a)} \tag{13}$$

$$\psi=\tan^{-1}\frac{2\pi xa'}{J(1+a)} \tag{14}$$

From equations (4) and (13)

$$\tan\psi=\frac{4\frac{dC_Q}{dx}}{\pi J^2x^3(1+a)^2}$$

But

$$\frac{C_Q}{J^2}=Q_c$$

Therefore

$$\tan\psi=\frac{4\frac{dQ_c}{dx}}{\pi(1+a)^2x^2} \tag{15}$$

Equation (15) expresses the relationship between the torque coefficient Q_c and the angle of twist in the propeller slipstream, which will be used later.

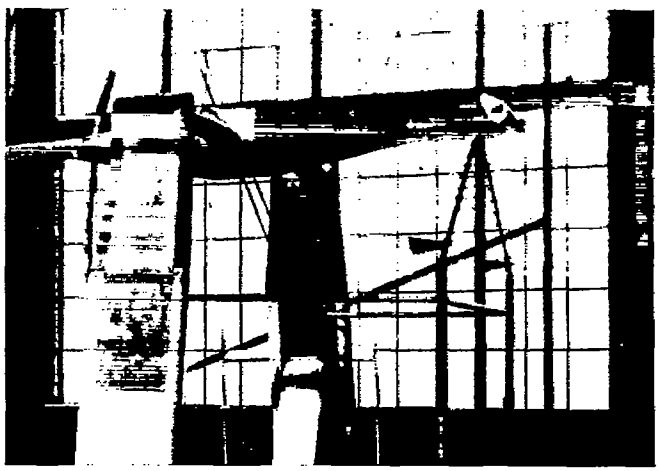

FIGURE 2.—Free-air body.

APPARATUS AND TESTS

The tests were conducted in the NACA 20-foot tunnel described in reference 3. Four body shapes were tested: a free-air body, a propeller-hub body, a body of revolution, and a body of revolution with an NACA cowling.

Figure 1 is a line drawing of the free-air body; a photograph of it is shown in figure 2. The propeller-hub body (fig. 3) consists of the propeller-shaft housing, which is 9.6 inches in diameter; a spinner band which turns with the propeller and which is mounted on a floating frame; and a spinner mounted on the fixed frame. Figure 4 shows the body of revolution that houses the motor and the propeller shaft. Figure 5 shows the body of revolution with an NACA cowling, the maximum diameter of which is 20 inches. A model of a J–5 engine, composed of dummy wooden cylinders, was mounted inside the cowling. The body of revolution with the cowling will hereinafter be referred to as the "NACA cowling." The propeller, which had two blades, was a 4-foot model of Bureau of Aeronautics drawing No. 4412. The blade-form curves of the propeller are given in figure 6.

Simultaneous measurements were made of the total thrust and torque and of the differential thrust and torque along the radius. The method of measuring the differential thrust and torque from measurements in the propeller wake was the same as used in reference 2.

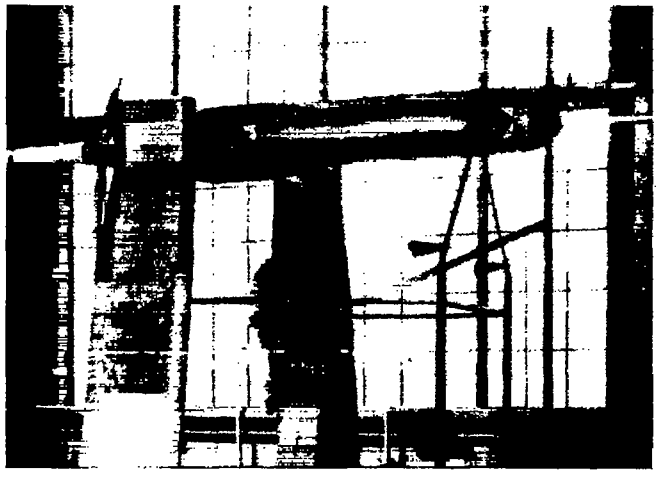

FIGURE 3.—Propeller-hub body.

The position of the tubes was such that yaw-head and total-head readings were observed at 22.2, 33.3, 44.4, 55.6, 66.7, 77.8, and 88.9 percent of the propeller radius from the center of the crankshaft.

RESULTS

The basic results of the force tests are given in figures 7 to 10. The efficiency envelopes for the four

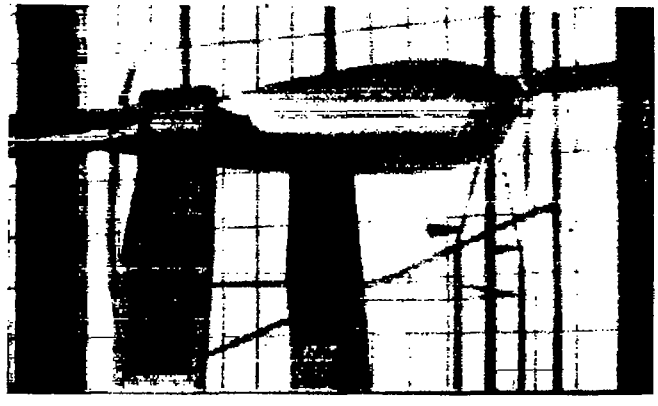

FIGURE 4.—Body of revolution.

body shapes are compared in figure 11. The efficiency obtained with the propeller-hub body is about 6 percent greater than that with the free-air body and this increase is due to the elimination of the drag of the propeller hub and the inner portion of the blade shanks by covering them. The spinner covered two-tenths of the propeller blade; the shaft housing had the same diameter as the spinner but was mounted on the fixed frame. In the case of a propeller mounted on a long shaft ahead of a body, the difference between the drag

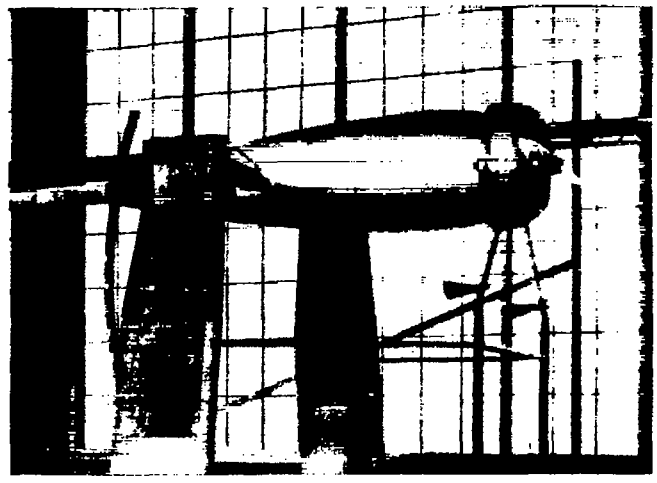

FIGURE 5.—Body of revolution; NACA cowling.

of the propeller hub and the spinner would be realized in the propeller efficiency.

The efficiency obtained with either the body of revolution or the NACA cowling is not the true, but the

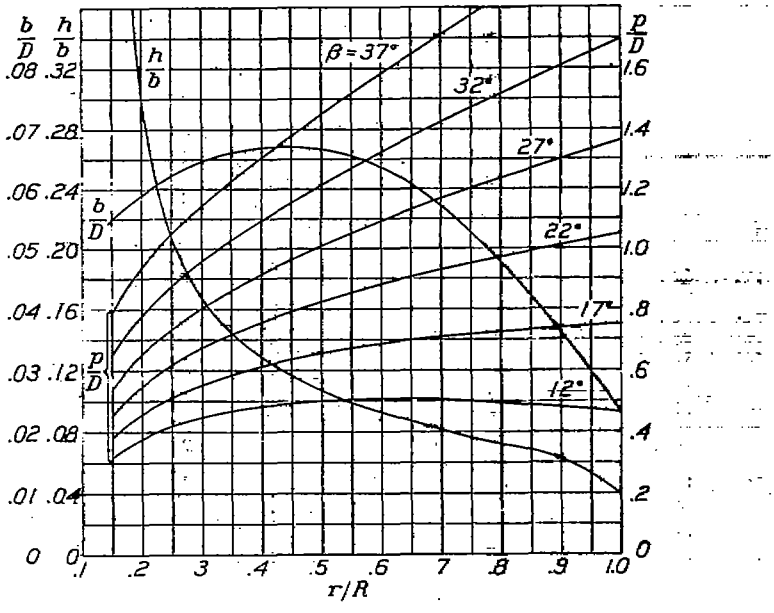

FIGURE 6.—Propeller blade-form curves. D, diameter; R, radius to the tip; r, station radius; b, section chord; h, section thickness; p, geometric pitch; β, blade angle of $0.75R$.

apparent, propeller efficiency. The propeller output used to compute the apparent efficiency was TV, whereas, the thrust was obtained in a region of velocity u_0 and the useful work per unit time was u_0T. The change from apparent efficiency to true efficiency will be discussed later.

Figures 12 to 15 give the thrust-gradient and the torque-gradient curves for the propeller-hub body. The curves are given only to $0.2R$ because the inner two-tenths of the propeller blades was covered by the propeller-hub body. The thrust-gradient curves for the other body shapes in the subsequent figures are also terminated at $0.2R$ because no pressure readings were taken inside that radius.

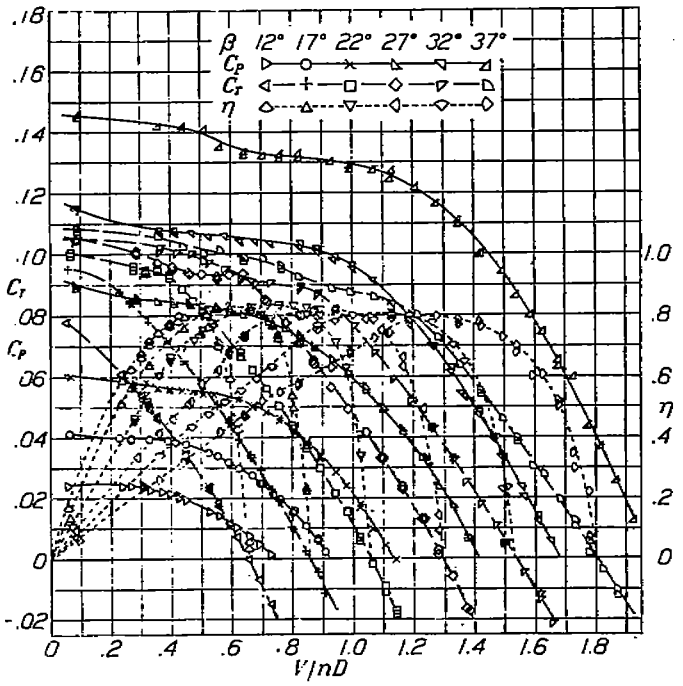

FIGURE 7.—Curves of C_T, C_P, and η against V/nD for free-air body

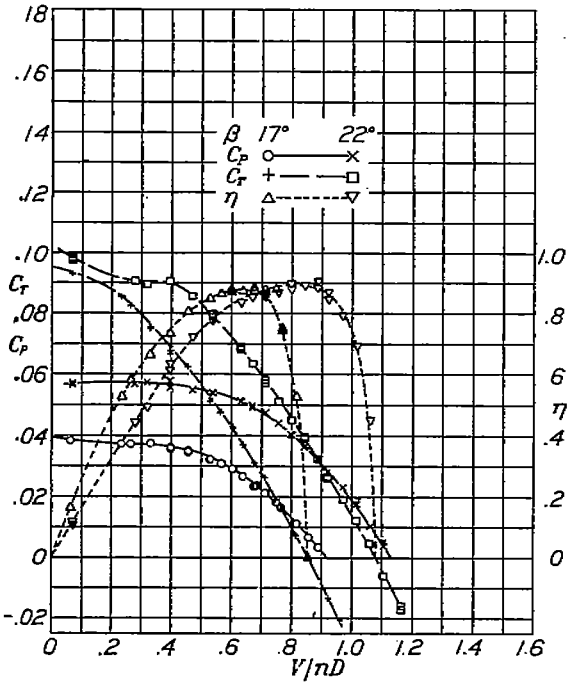

FIGURE 8.—Curves of C_T, C_P, and η against V/nD for propeller-hub body.

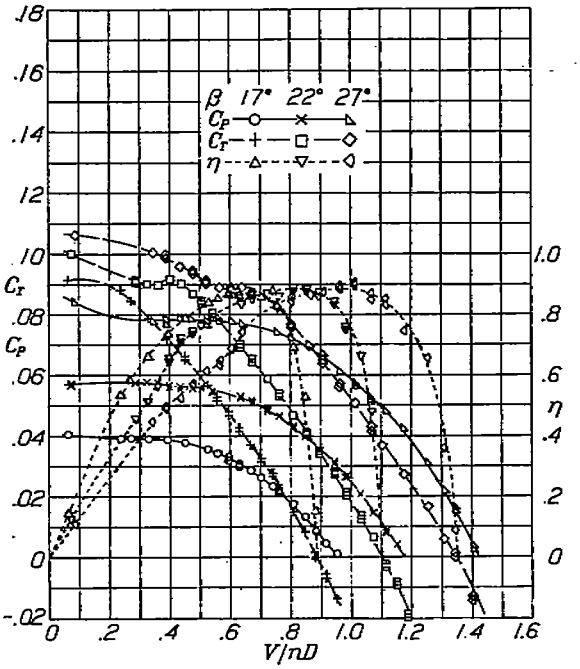

FIGURE 9.—Curves of C_T, C_P, and η against V/nD for body of revolution.

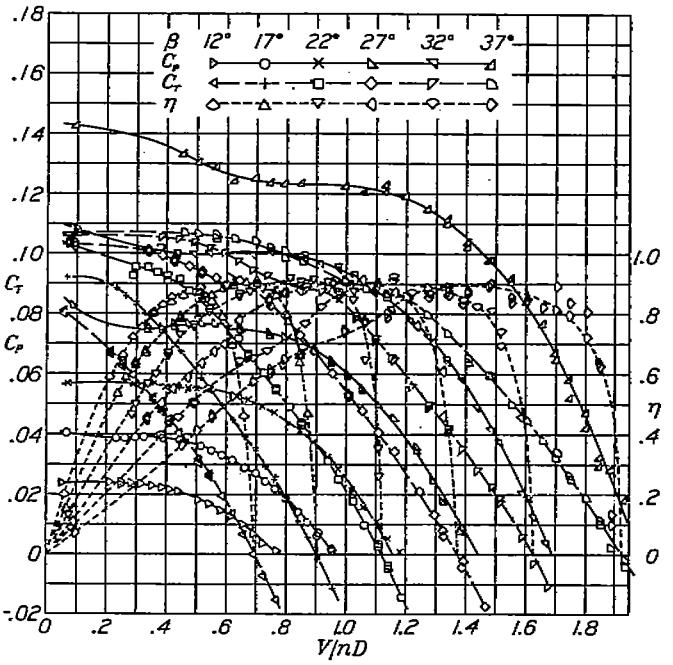

FIGURE 10.—Curves of C_T, C_P, and η against V/nD for NACA cowling.

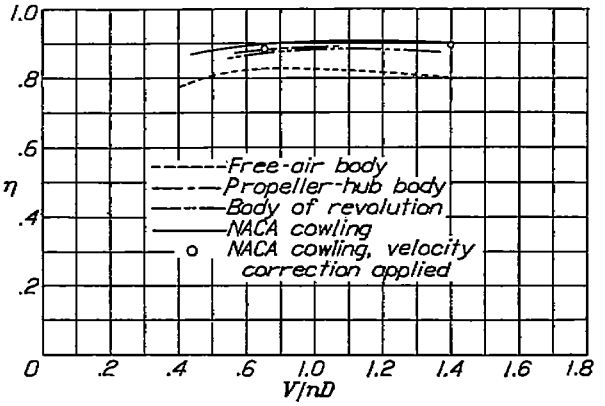

FIGURE 11.—Comparison of apparent propeller efficiency envelopes for four body shapes

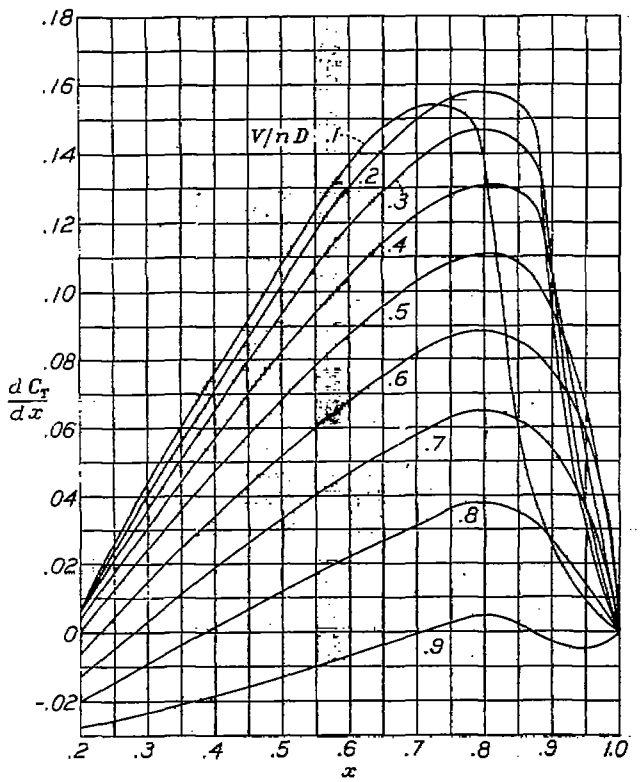

FIGURE 12.—Curves for dC_T/dx against x for propeller-hub body. β, 17°.

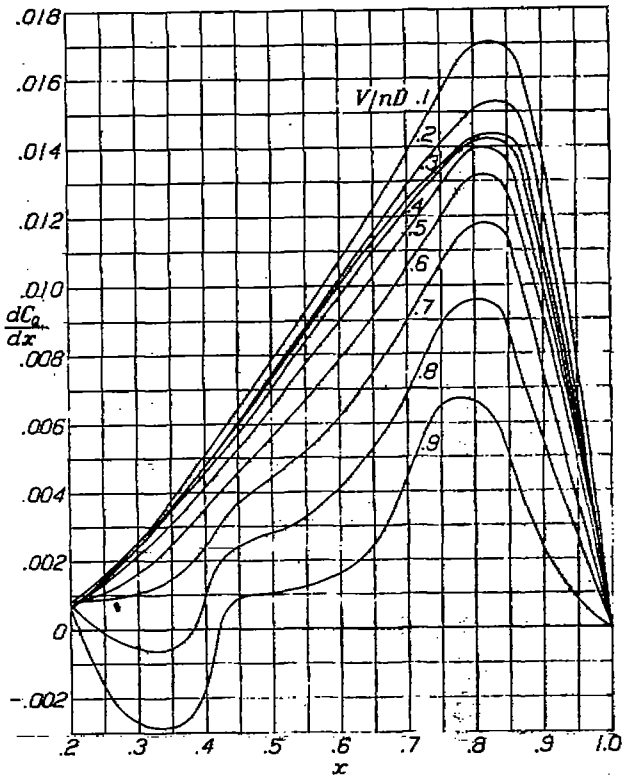

FIGURE 13.—Curves for dC_Q/dx against x for propeller-hub body. β, 17°.

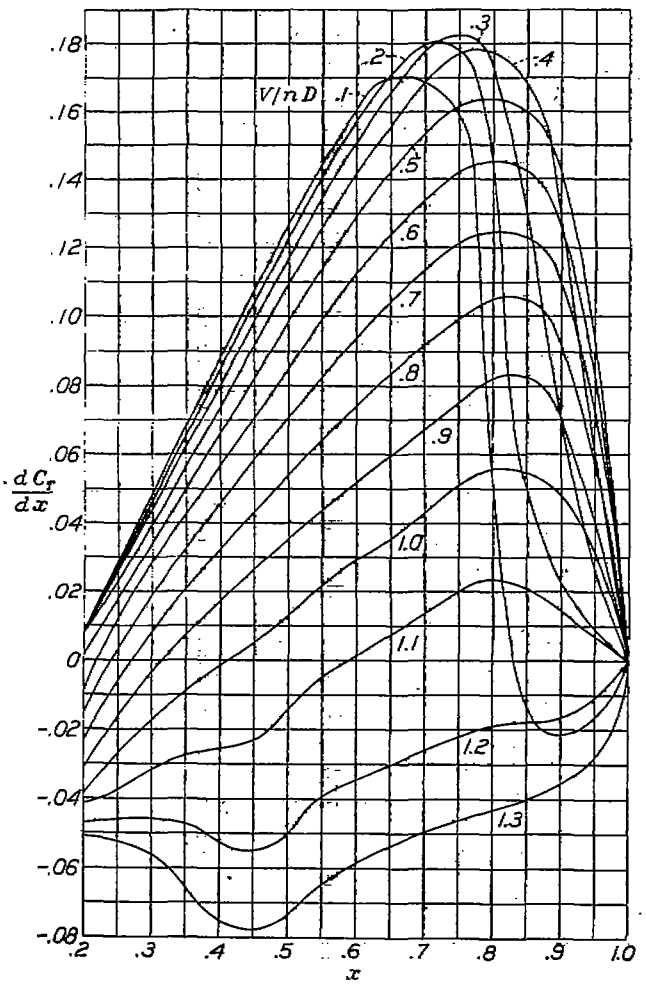

FIGURE 14.—Curves for dC_T/dx against x for propeller-hub body. β, 22°.

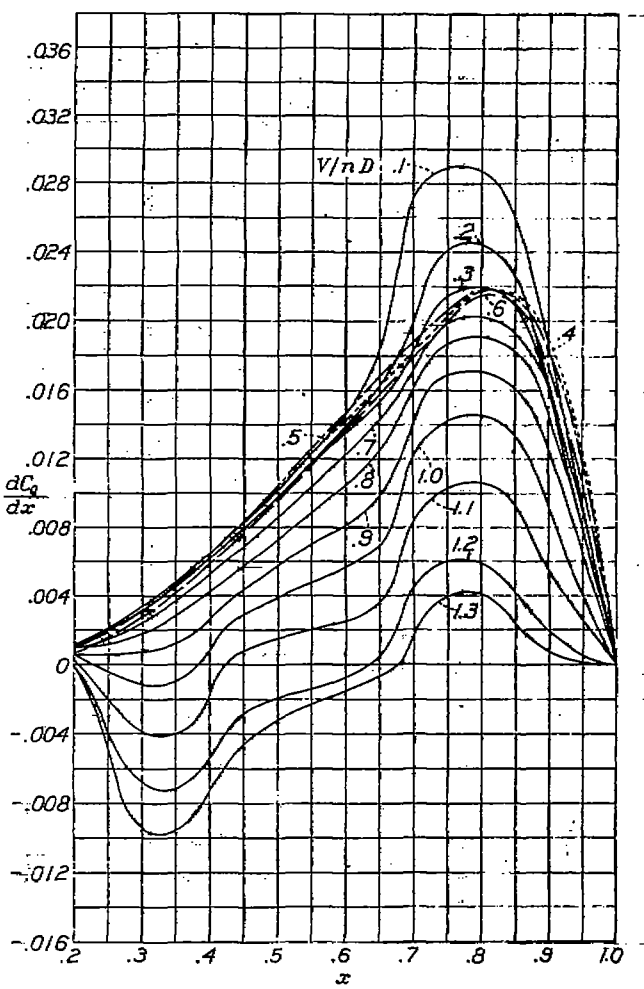

FIGURE 15.—Curves for dC_Q/dx against x for propeller-hub body. β, 22°.

Figure 16 gives a comparison of the thrust coefficients for the propeller-hub body obtained from the force measurements and the total-pressure measurements. The values for the total-pressure measurements are a direct integration of the thrust-distribution curves in

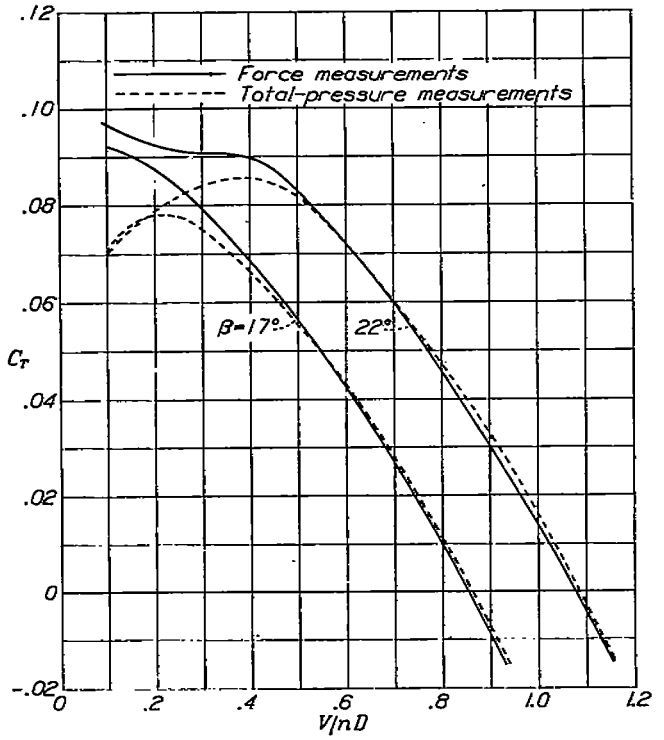

FIGURE 16.—Comparison of thrust coefficients from force measurements and total-pressure measurements. Propeller-hub body.

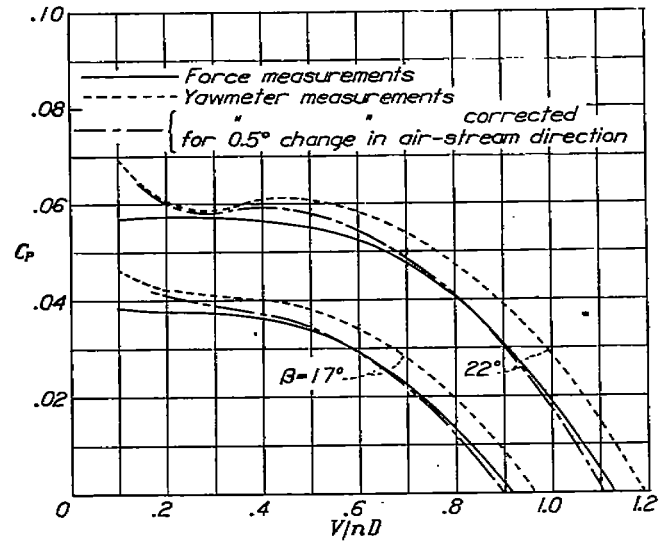

FIGURE 17.—Comparison of power coefficients from force measurements and yawmeter measurements. Propeller-hub body.

figures 12 and 14. No corrections were necessary to these integrated values because the propeller-hub body shielded the inner part of the propeller. The large differences at low values of V/nD are caused by an error in the measurement of total pressure behind the propeller due to large angles of slipstream yaw.

A comparison of the values of power coefficient obtained from the force and the yawmeter measurements is given in figure 17. Since the yawmeter measurements indicate yaw in the slipstream at zero input power to the propeller, as shown by the discrepancy at zero measured power, it is concluded that the direction of the main air stream was changed owing to the presence of the propeller. This same effect was noted in a series of tests on a different test set-up using full-scale propellers. Figure 17 shows the effect on the integrated power coefficient of applying a constant correction corresponding to 0.5° angle of yaw. This small change in the direction of the tunnel air stream brings the integrated results into substantial agreement; these corrected values are used in the further

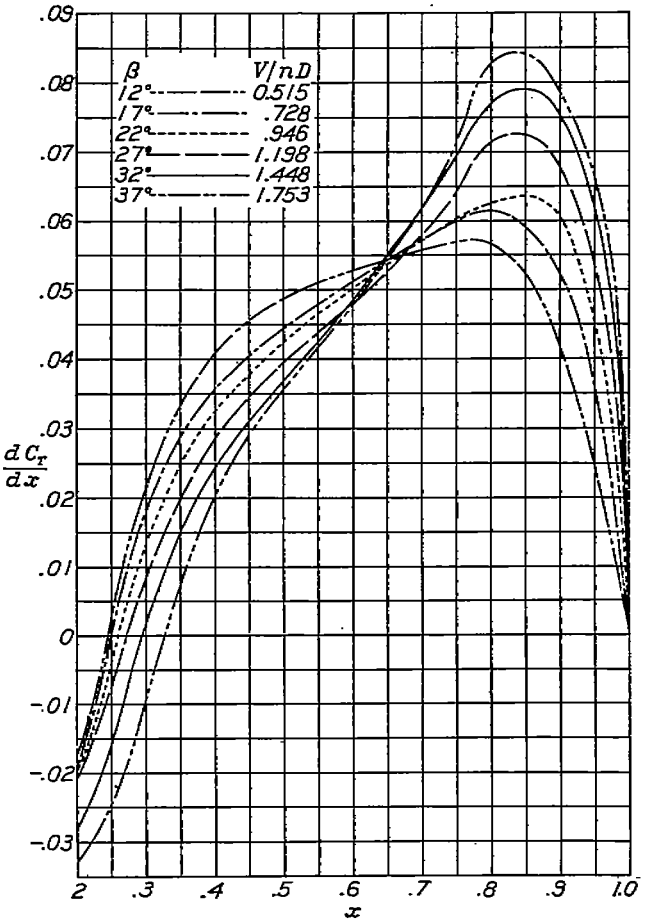

FIGURE 18.—Variation in thrust distribution with propeller blade-angle setting at a constant value of C_T of 0.0320. NACA cowling.

analysis of the propeller characteristics. The air-stream correction apparently varies with the propeller operating condition because the constant correction of 0.5° overcorrects the values for high values of V/nD and undercorrects the values for low values of V/nD. The angle of the air stream ahead of the propeller is probably also changed by the body size and shape.

The comparisons of force and integrated measurements are valuable as an indication of the accuracy of the distribution curves. The propeller-hub body

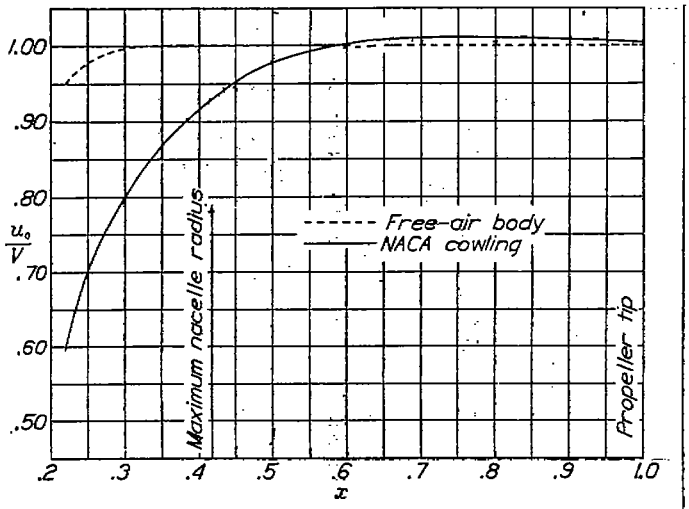

FIGURE 19.—Velocity distribution in plane of propeller (propeller removed). V, 93 miles per hour.

furnishes the best opportunity to determine this accuracy, no corrections being necessary to put the integrated and the measured results on an equal basis because of the hub drag. The fact that the integrated power coefficients need a correction to bring them into agreement with the measured power coefficients indicates that the integrated power measurements are quantitatively inaccurate. Inasmuch as a constant correction to the angle of yaw of the tunnel air stream brings the results into substantial agreement, the distribution of the torque along the blade is believed to be sufficiently accurate for use in further analysis.

Figure 18 shows the variations in thrust distribution with propeller blade-angle setting for the NACA cowling at a constant value of C_T of 0.0320, which is approximately at peak efficiency for the blade-angle setting of 12°. The effect on the thrust distribution caused by the change in the pitch distribution (fig. 6) is shown. As the blade-angle setting is increased, the slope of the pitch-distribution curve is increased, which causes the thrust to move toward the tip of the propeller.

The velocity distribution in the plane of the propeller with the propeller removed is shown in figure 19 for two body shapes.

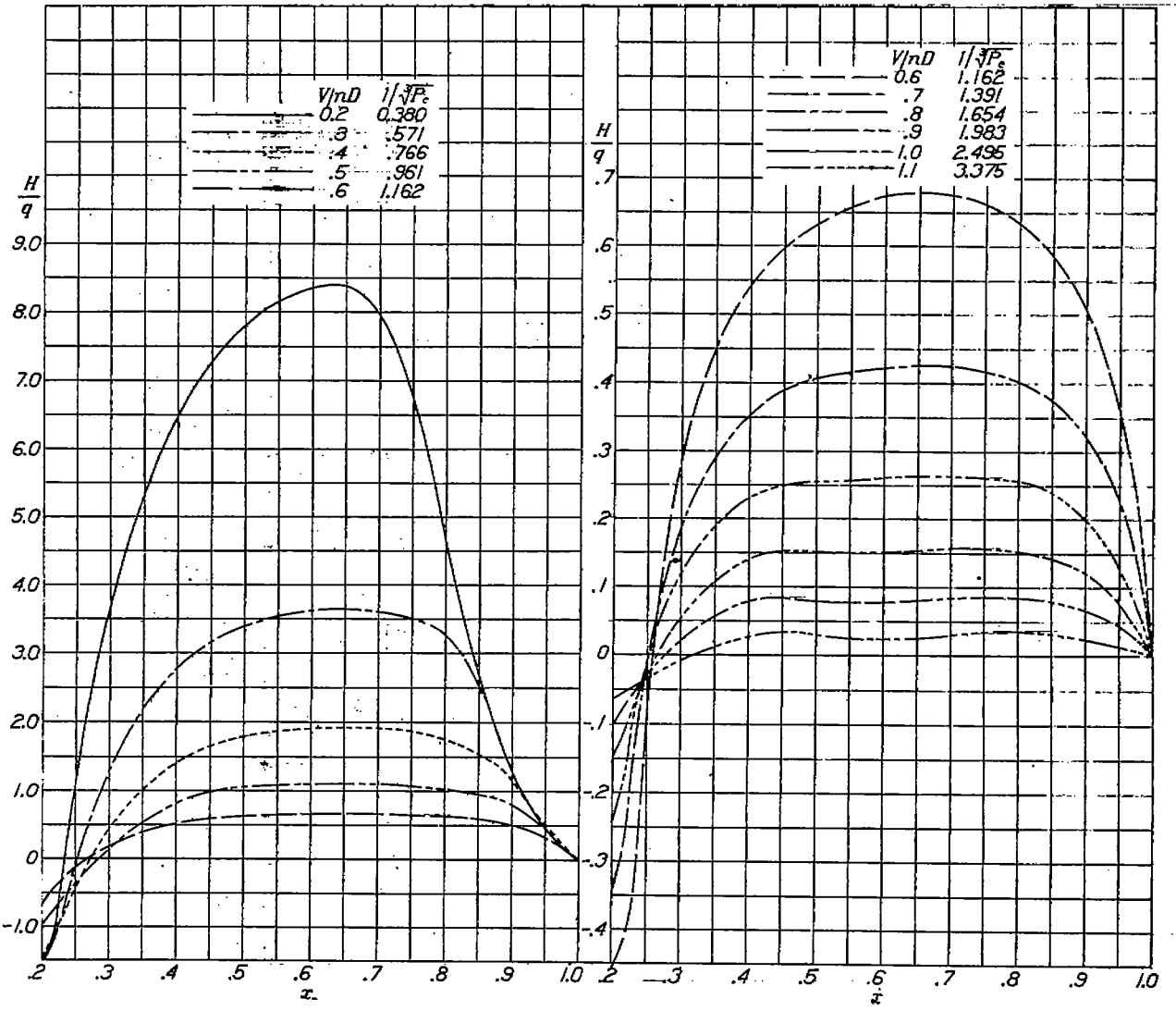

FIGURE 20.—Curves of H/q against x for NACA cowling. β, 22°

DISCUSSION

TOTAL PRESSURE DUE TO THE PROPELLER

The effect of the propeller slipstream on the body behind the propeller may be studied by determining the increase in total pressure due to the propeller. This increase in pressure divided by the dynamic pressure of the undisturbed air stream may be computed directly from the thrust-distribution curves and equation (5). Figure 20 shows the distribution of H/q along the radius for the 22° blade-angle setting with the NACA cowling. The magnitude of H/q will remain essentially the same for equal values of $1/\sqrt[3]{P_c}$ regardless of blade-angle setting; the maximum value, however, will shift toward the tip as the blade-angle setting is increased. For optimum design the shift will be smaller than is shown for this test propeller. The values of V/nD are shown on the curves for comparative purposes, but it must be kept in mind that the curves of H/q against V/nD can be used for only the blade-angle setting given.

The magnitude of the increase in total pressure in the region in front of the body permits a rough approximation of the increase in body drag due to the propeller slipstream, provided that the type of flow over the body is not critically affected by the slipstream. If the slipstream changes the flow over the body, the change in drag cannot be predicted.

The curves of H/q are useful in indicating the increase in total pressure that can be obtained in a scoop or other air intake located behind the propeller.

Because of the increase in total pressure that can be obtained behind good propeller blade sections, the cooling of engines should be taken into acount in the design of the inner sections, especially when the engines are mounted in open-nose cowlings.

PROPELLER EFFICIENCY IN THE REGION OF REDUCED VELOCITY

Computation of the true propeller efficiency from the apparent propeller efficiency for the NACA cowling can be made by the use of thrust-distribution curves (fig. 19), equation (7), and u_0/V data. Figure 21 illustrates the results of calculation for blade-angle settings of 17° and 37° at $0.75R$ for the peak-efficiency points. The ratio of the areas under the curves gives the factor by which the apparent propeller efficiency must be multiplied to give the true propeller efficiency. The correction amounts to approximately 2 percent for the 17° blade-angle setting but disappears for the 37° blade-angle setting because of the shift of the thrust distribution from the low-velocity region to the high-velocity region near the tip. The results of this correction to the peak efficiencies of the two blade-angle settings are shown as points in figure 11.

The disappearance of this correction is particularly applicable to the test conditions and should not be applied as a function of blade-angle setting for other conditions.

VELOCITY INCREASE DUE TO THE PROPELLER

In order to study the inflow velocity ahead of the propeller, survey measurements were made with and without the propeller operating. Figure 22 shows the results of these measurements for two body shapes with the propeller operating near peak efficiency at a blade-angle setting of 22° at $0.75R$. For the NACA cowling, the maximum inflow velocity at the center line of the propeller is 7 percent of the free-stream velocity and is only 2 percent at a distance one-third of the propeller diameter ahead of the propeller. These curves also show how the NACA cowling increases the

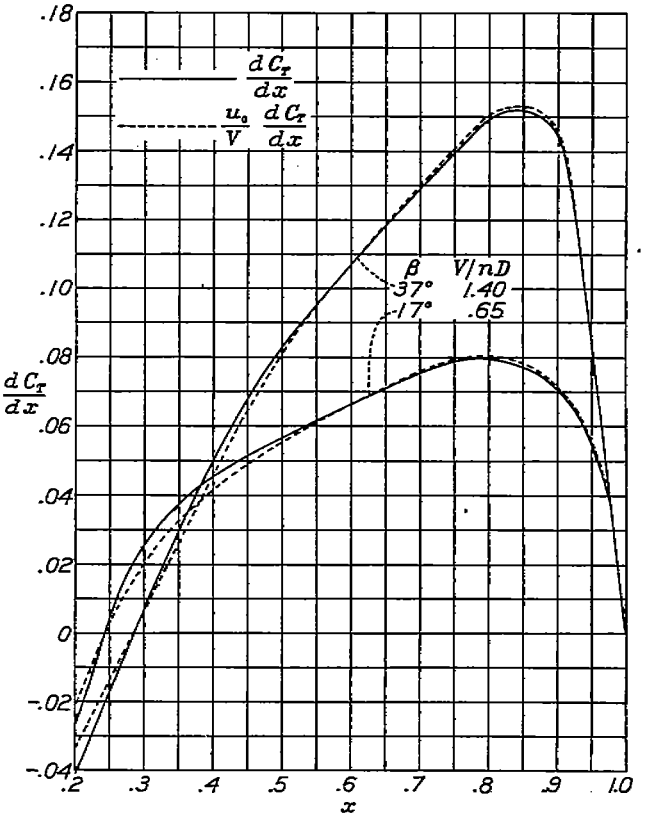

FIGURE 21.—Example illustrating the method of determining true propeller efficiency in presence of body. NACA cowling.

angle of attack of the propeller sections by decreasing the axial velocity over these inner sections.

ANGLE OF TWIST IN THE SLIPSTREAM

A knowledge of the magnitude of the angle of twist ψ in the propeller slipstream is helpful in the interpretation of the action of airplane parts, such as intake scoops and wing fillets. The angle of twist immediately behind the propeller plane may be calculated from equation (14). This angle of twist will vary with the distance from the propeller plane. Two separate effects that change the angle of twist are: The conversion of static pressure into dynamic pressure increases the axial component of the velocity, which reduces the angle of twist, and the contraction of the slipstream combined with the change of the cross section of the afterbody in

the slipstream changes the radius of the streamlines and, consequently, changes the angular velocity of the slipstream. The effect of speeding up the axial velocity amounts to only a small change in the angle of twist. If the propeller is operating in front of a blunt body like an NACA cowling, the angle of twist in the slipstream close to the surface is less than that calculated immediately behind the propeller. This difference in the angle of twist is due to the acceleration of the air going over the cowling and to the increase in the radius of the streamlines, which decrease the angular velocity of the air.

Figure 23 shows the change, at various operating conditions, of the angle of twist with x in the propeller slipstream immediately behind the propeller computed for two blade-angle settings. Equation (15) gives the angle of twist in the propeller slipstream as a function of the torque coefficient Q_c. An estimate of the angle of twist in the slipstream for any propeller-body combination may be obtained by computing Q_c for the propeller operating condition desired and by using figure 23 to estimate the angle. It must be kept in mind, however, that the distribution of twist along the radius varies with pitch distribution, body shape, and operating condition; consequently, an exact value of the angle of twist for other propeller-body combinations cannot be obtained from figure 23.

For the 22° blade-angle setting, the maximum propeller efficiency occurs at $V/nD=0.803$ or a value of $1/\sqrt{Q_c}$ of 10. It may be seen from figure 23 (b) that the angle of twist for this operating condition is less than 3°. This angle of twist is representative of the value obtained with a propeller operating in the cruising or the high-speed condition of flight.

DISPOSITION OF PROPELLER POWER

The disposition of the power input to the propeller with the propeller-hub body is given for the 17° blade-angle setting in figure 24 (a) and for the 22° blade-angle setting in figure 24 (b). The percentage of power between the propeller-efficiency curve and unity represents the losses of the propeller. The thrust-distribution and the torque-distribution curves in conjunction with equations (9) and (11) permit the calculation of the energy going into the propeller slipstream in the form of axial and rotational velocity. Equation (9) may be rewritten as

$$\frac{E_a}{P}=\frac{\eta}{C_T}\int_0^1 a\frac{dC_T}{dx}\,dx$$

It may be seen that E_a/P, to the first order, is proportional to the product of η and a.

Equation (3) may be rewritten in the form

$$a=\frac{-1+\sqrt{1+\frac{1}{2x}\frac{dT_c}{dx}}}{2}$$

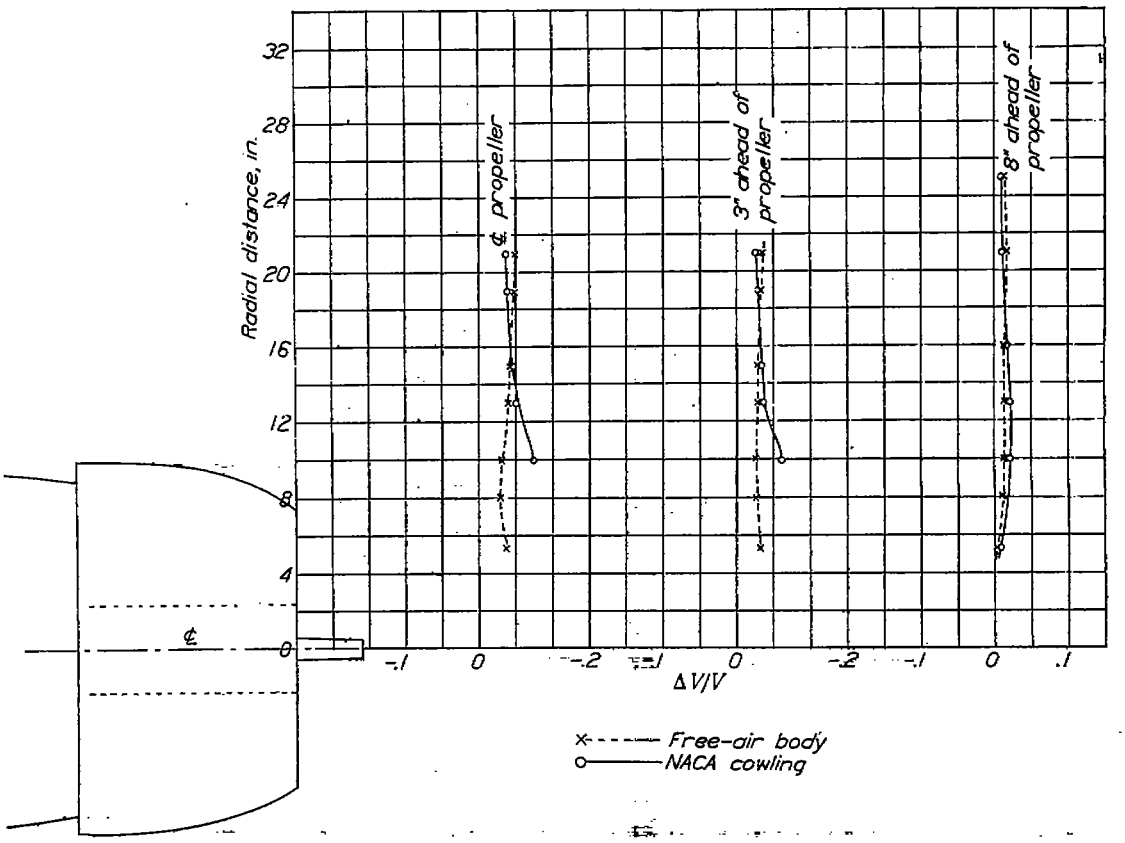

FIGURE 22.—Fractional increase in velocity due to propeller. β, 22°; V/nD, 0.895.

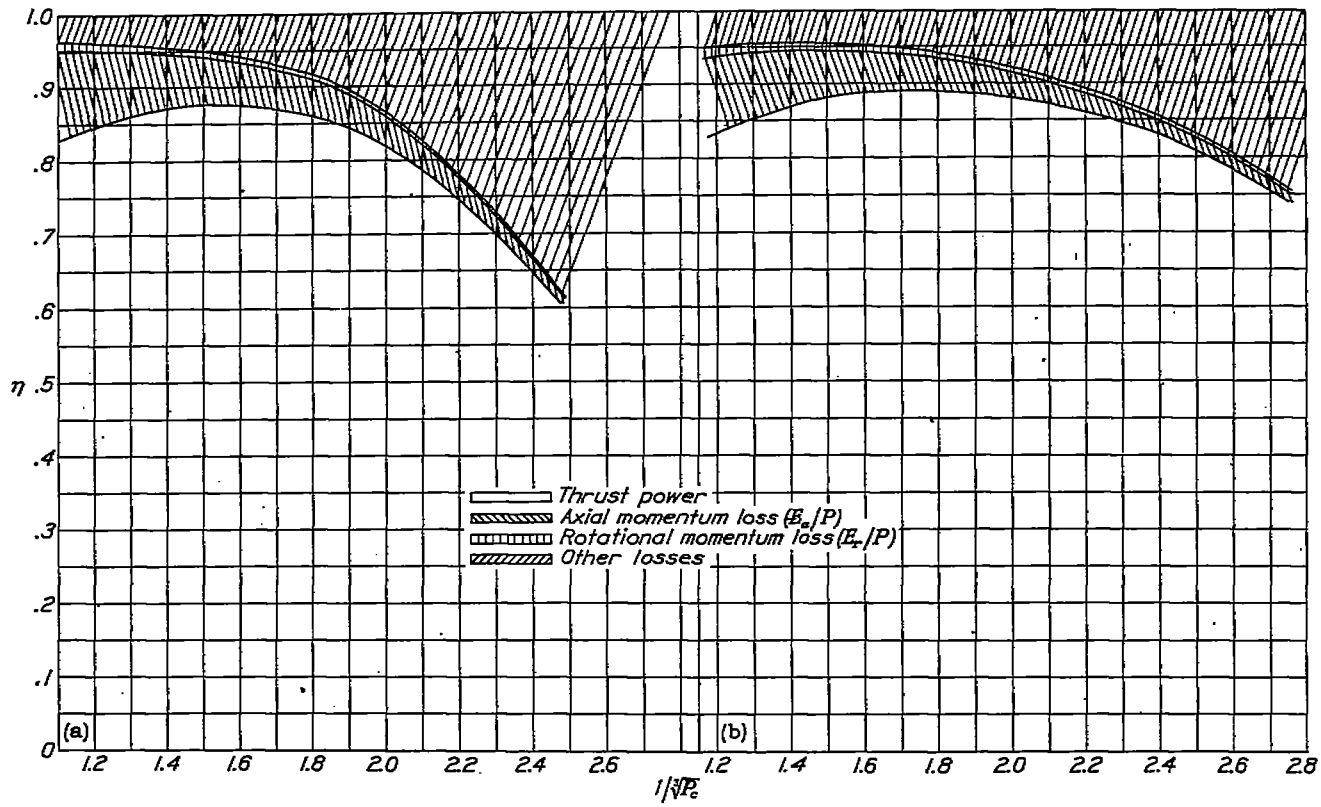

(a) β, 17°. (b) β, 22°.

FIGURE 24.—Disposition of propeller input power. Propeller-hub body.

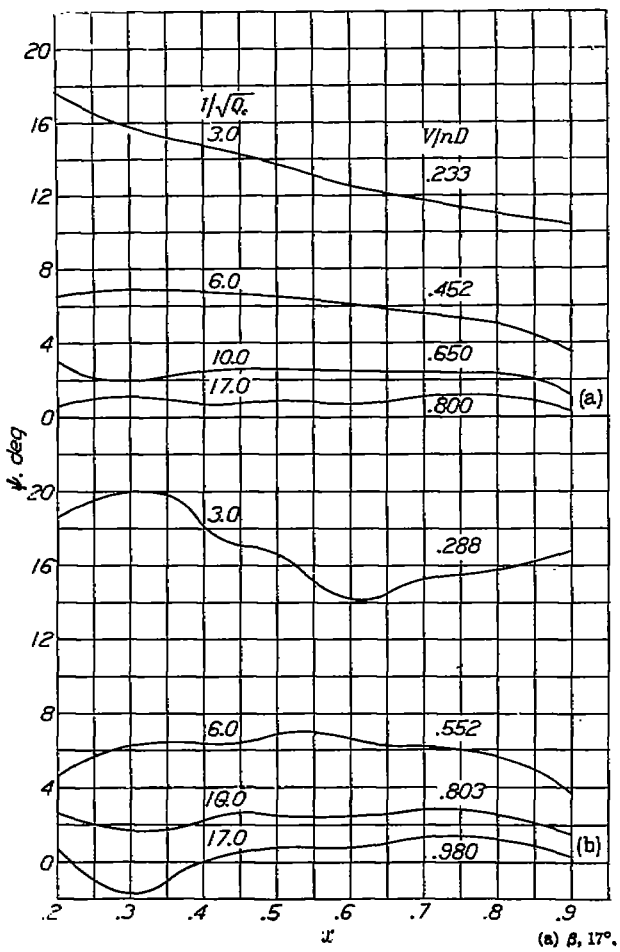

(a) β, 17°.
(b) β, 22°.

FIGURE 23.—Curves of angle of twist in the slipstream. Propeller-hub body.

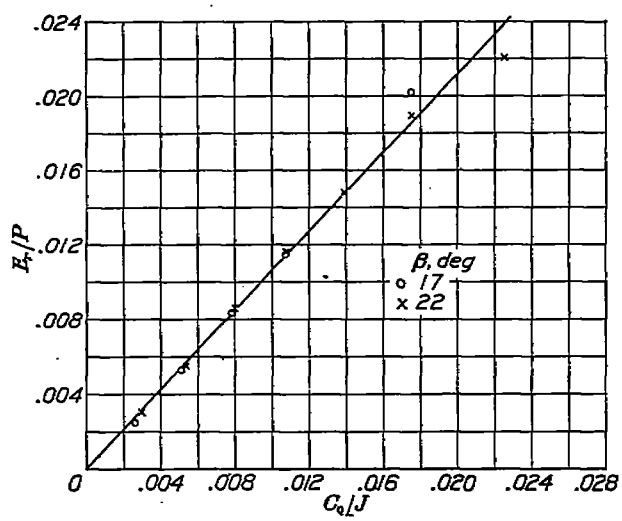

FIGURE 25.—Experimental curve showing relationship of E_r/P to C_Q/J.

which shows that a is a direct function of dT_c or that E_a/P is a function of T_c and η, if changes in the distribution of thrust are neglected.

From equation (11a) it is seen that the fractional part of the power going into rotational velocity in the wake is proportional to a'.

Equation (4) may be written in the form

$$a' = \frac{dC_Q}{dx}\frac{2}{\pi^2 J x^3(1+a)}$$

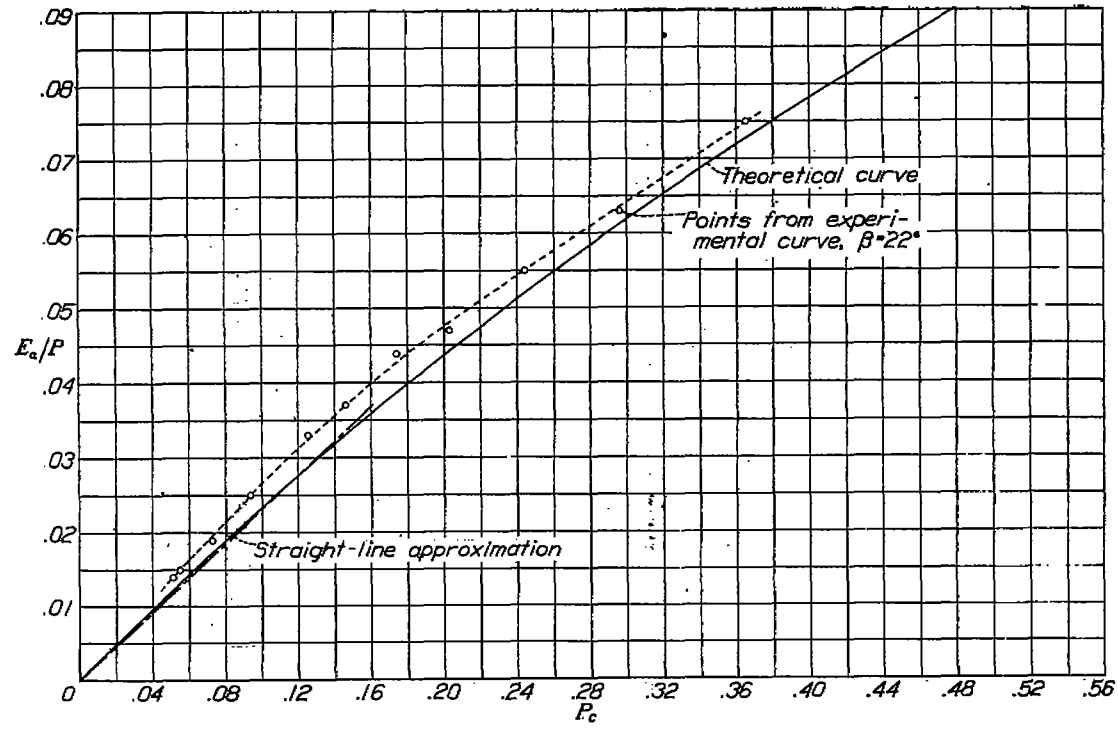

FIGURE 26.—Relationship between P_c and axial energy in the propeller wake.

If the small effect of the factor $(1+a)$ is neglected, a' is proportional to $\frac{dC_Q}{dx}\frac{1}{J}$ or E_r/P is proportional to C_Q/J, if the effect of torque distribution is neglected. Figure 25 is a plot of E_r/P as a function of C_Q/J for the 17° and the 22° blade-angle settings of the propeller-hub body.

From figure 25

$$E_r/P=C\frac{C_Q}{J}$$

where $C=1.06$ for the test propeller at the blade angles tested.

The value of C in the foregoing equation primarily depends on the torque distribution and will rapidly increase for a poor torque distribution.

ANALYSIS OF PROPELLER POWER LOSSES

FRACTIONAL PART OF POWER LOST IN AXIAL VELOCITY

Figure 26 gives the theoretical relationship between the coefficient P_c and the power lost in axial velocity in the wake of the propeller for ideal propeller efficiency. (See reference 1, p. 189.) The high-speed range of propeller operation ($P_c=0$ to $P_c=0.16$ or $1/\sqrt[3]{P_c}=\infty$ to $1/\sqrt[3]{P_c}=1.85$) may be approximated by a straight line through the origin. This result shows that for this range E_a/P is proportional to the power disk loading, that is, if the power is doubled, the loss is doubled. The experimental curve for $\beta=22°$, obtained with the test propeller, has also been plotted in figure 26. It may be noted that the agreement is very good; the difference in no case exceeds one-half of 1 percent of the total power lost.

The difference between theory and experiment shown by figure 26 may be due to one of two effects. First, any change in the thrust distribution from the optimum for ideal efficiency will result in a small change in axial energy in the wake. For example, if thrust is added where the axial interference factor a is larger than the average a for the entire propeller, the fractional power lost in the axial velocity will be increased; whereas, if thrust is added where a is smaller than the average a for the entire propeller, the loss will be decreased. Second, a decrease in propeller efficiency at a given P_c will decrease the proportion of power in axial velocity in the propeller wake, and an increase in propeller efficiency will have the opposite effect. It is thus seen that the two effects tend to counteract each other and that the theoretical curve gives a fair approximation of the value of E_a/P in the wake of a normal propeller. If a more exact result is required, the known thrust distribution and the known propeller operating conditions must be substituted in equation (9).

FRACTIONAL PART OF POWER LOST IN ROTATIONAL VELOCITY

It has been shown that a good approximation of the axial-energy loss encountered in high-speed propeller operation may be obtained from the theoretical curve. The rotational-energy loss is very greatly affected by

changes in the distribution of propeller loading, however, and no theoretical estimate can be made of this energy loss from the total power of the propeller without a knowledge of the torque distribution.

The total torque at peak efficiency for three types of propeller is given in figure 27, which is a plot of C_P at V/nD for peak efficiency and the peak-efficiency envelopes against V/nD. One of these, the two-blade Goldstein propeller (reference 4) was specially designed to correspond to the "minimum energy loss" condition of Betz, for a certain relation between blade angle and working condition. The hub and the inner portion of the propeller were covered to a radius of $0.27R$ by a long cylindrical body with a streamline nose and tail that was supported free of the propeller. The propeller efficiency was measured. The results for propeller C on nose 4 were taken from reference 5. Nose 4 extended through the propeller disk in the form of a large spinner and covered the radius to approximately $0.25R$. Propeller C is Bureau of Aeronautics drawing No. 5868–9, is 10 feet in diameter, and has three blades. The *propulsive* efficiency was obtained from tests in reference 5 and is plotted in figure 27. Propeller E (reference 6) was a 3-foot-diameter model of standard Navy plan form. No spinner was used, the propeller being entirely exposed on a long shaft.

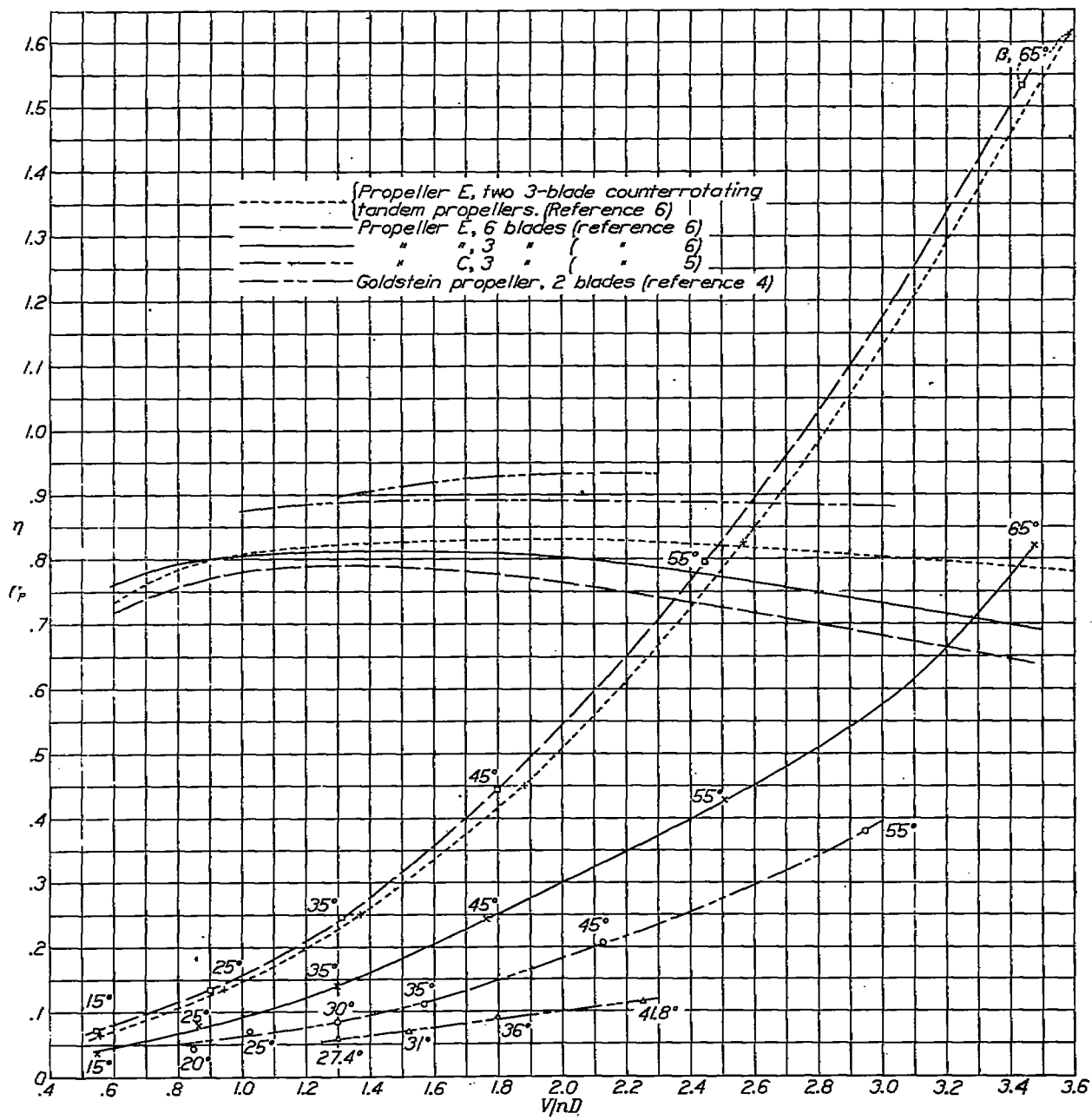

FIGURE 27.—Efficiency-curve envelopes and values of C_P at V/nD for peak efficiency.

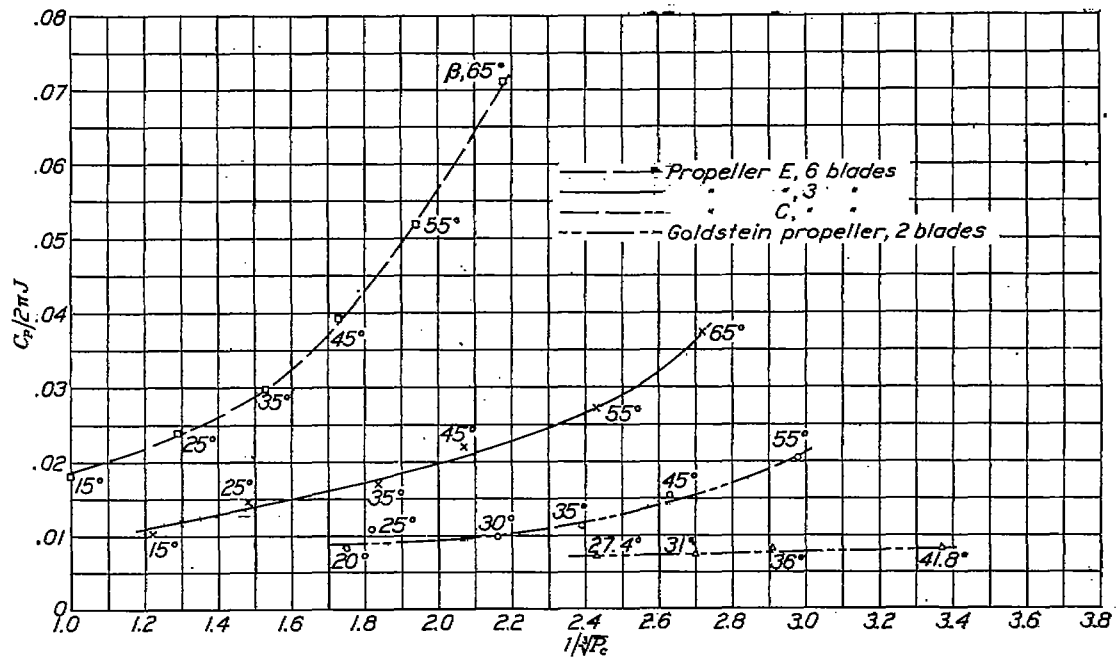

FIGURE 28.—Relationship between $1/\sqrt[5]{P_c}$ and $C_P/2\pi J$ at V/nD for peak efficiency

The *propeller* efficiency was measured in the Stanford tests reported in reference 6. Propeller E was tested as a three-blade, a six-blade, and two three-blade counterrotating tandem propellers.

The V/nD for peak efficiency for a given blade-angle setting is the lowest for propeller E and the highest for

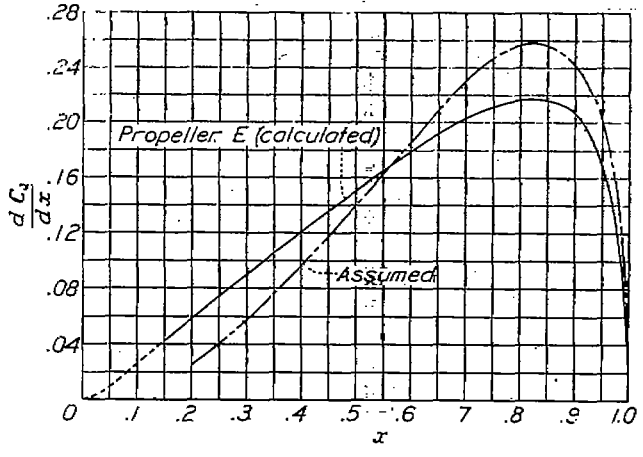

FIGURE 29.—Torque-gradient curves. β, 65°.

the Goldstein propeller. The order is the same for the efficiency-envelope curves, which demonstrates the fact that any increase in propeller losses (decrease in efficiency) increases the value of the power loading at which peak efficiency for a given blade angle will occur for a given propeller. There are two obvious reasons why the losses of propeller E were the greatest. First, the propeller hub and the blade shanks, which were exposed to the air stream on propeller E, gave excessive losses in drag that could have been considerably reduced with a spinner. Second, the load distribution for the high blade angles was very poor for propeller E, which gave a large increase in the rotational energy of the slipstream. The counterrotating tandem propellers considerably reduce the rotational-energy losses, and it is seen that V/nD is slightly higher for peak efficiency at low blade-angle settings and that the difference increases with blade angle. The results of figure 27 have been replotted in a different form in figure 28. Note that $C_P/2\pi J$ remains approximately constant with power loading for the Goldstein propeller but rapidly increases for propeller E.

In the formula

$$E_r/P = C\frac{C_P}{2\pi J}$$

if C remained constant for all blade angles of a given propeller, the values of $C_P/2\pi J$ from figure 28 could be directly used in obtaining E_r/P for the propeller under consideration. But, since the distribution of torque along the blade did not remain optimum for either propeller C or E, it was necessary to evaluate C for the test conditions.

A calculation of the thrust and the torque distributions for the test conditions of propeller E was computed from the airfoil characteristics. The Goldstein corrections were applied to the results and the values were adjusted to give the correct value of C_P for peak efficiency. From these distributions E_r/P and C have been evaluated. It must be realized that this method gives only an approximation of the thrust and the torque distributions and that the exact distributions must be known to obtain the exact rotational-energy loss.

A sample curve of the torque distribution at peak propeller efficiency from such calculations is given for $\beta=65°$ for propeller E in figure 29. A revised torque distribution that gives the same total torque is included in the same figure. In the revised distribution it is assumed that the propeller hub and the inner two-tenths of the blades are covered with a spinner. The torque curve would thus be cut off at the $0.2R$ station. The computed values of $a'\frac{dC_Q}{dx}$ for the two torque distributions of figure 29 are shown in figure 30. For the three-blade propeller E at peak efficiency for $\beta=65°$, $C_Q=0.1305$ and, for this condition, 11 percent of the total power was lost in rotational energy in the wake. Only 4.3 percent of the power would be lost in rotational energy for the assumed distribution that has equal total power. The curve shows the great importance of unloading the inner sections of the propeller at high blade angles. It also shows that a spinner will eliminate a large percentage of the rotational-energy loss caused by improper load distribution.

Figure 31 gives the variation of the term $\dot{C}$ with blade-angle setting computed for propeller E. The rapid rise in C at high blade angles is due to the poor torque distribution. The value of C at $\beta=65°$ for this distribution is 2.94 but is only 1.15 for the assumed distribution, which is approximately the same value as was obtained at the 25° blade-angle setting. The torque distribution was computed for only three blade angles, 25°, 45°, and 65°, but the curve as shown in figure 31 was used in obtaining C to compute the rotational-energy losses for other blade angles from the relation $E_r/P=C\frac{C_P}{2\pi J}$. The value of E_r/P for propeller C was obtained from thrust and torque distribution curves of unpublished data. The thrust and the torque distribution curves for the Goldstein propeller were

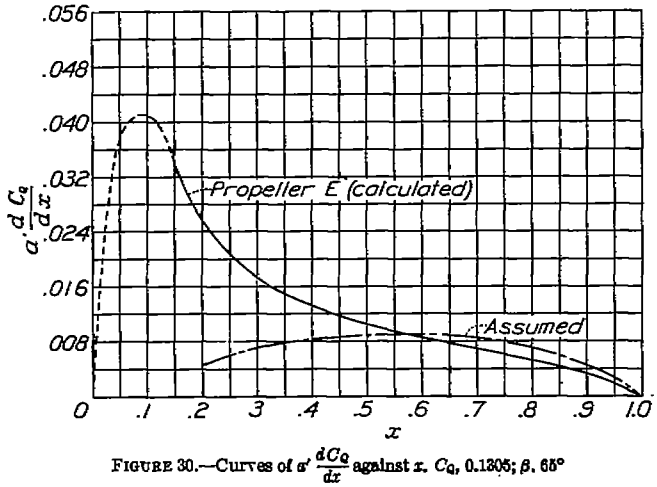

FIGURE 30.—Curves of $a'\frac{dC_Q}{dx}$ against x. C_Q, 0.1305; β, 65°

computed for a blade-angle setting of 41.8°; C as computed was 0.98. It is believed, therefore, that $C_P/2\pi J$ gives a close approximation of E_r/P for the Goldstein propeller over the entire range, and this value is used in the comparisons of the following sections.

Figure 32 gives the theoretical curve of E_a/P and the curves of E_r/P for the three types of propeller plotted against $1/\sqrt[3]{P_c}$. The data for the curves for the three-blade, the four-blade, and the six-blade Goldstein propellers were computed on the assumption that at the same V/nD the power, and therefore the percentage of power, going into rotational energy is proportional to the number of blades. At low values of $1/\sqrt[3]{P_c}$ the chief loss of efficiency is due to the axia velocity in the propeller wake, but this loss rapidly decreases with an increase in $1/\sqrt[3]{P_c}$, becoming of the order of 1 percent at values $1/\sqrt[3]{P_c}$ corresponding to very high speeds. On the other hand, the loss in efficiency due to the rotational velocity is always small for a propeller of optimum design, being of the order of 1 percent for the low solidity two-blade propeller. The rapid rise in rotational-energy loss for propellers C and E is due to the poor load distribution on the inner radii of these propellers when set at high blade angles, the distribution being much worse for propeller E than for propeller C.

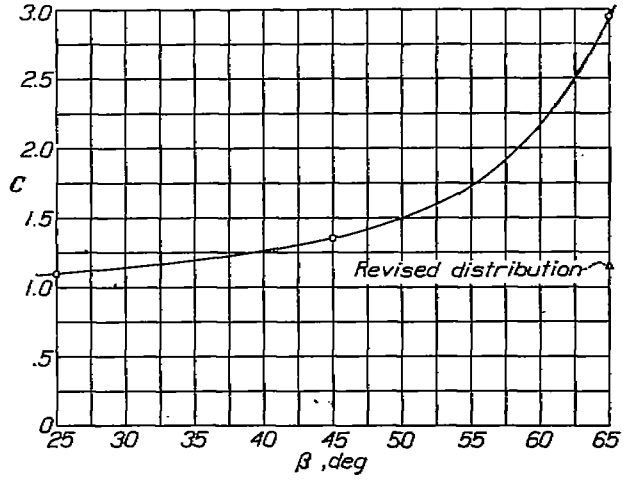

FIGURE 31.—Variation of C with blade angle for propeller E.

APPLICATION OF ANALYSIS TO COUNTERROTATING PROPELLERS

The fact that the rotational-energy loss is greatly dependent on the torque distribution of a propeller and that the rotational-energy loss may be increased many times by the use of a propeller with poor torque distribution makes it possible to show a large increase in efficiency by the use of counterrotating propellers with propellers that have poor torque distribution.

For any given propeller it is evident that there should be a balance between the axial-energy and the rotational-energy losses, which balance is represented by the point where the curves of axial-energy and rotational-energy losses cross in figure 32. At this point, then, there can be no gain in propeller efficiency by using counterrotating propellers of double solidity because, even if it is assumed that all the rotational-energy loss may be recovered, the axial-energy loss

will be doubled. At any blade-angle setting below this point, the efficiency of counterrotating propellers is less than the efficiency of a single propeller; above this point some gain may be expected. For example, suppose that two propellers, geometrically similar to propeller C, are operating independently of each other at a value of $1/\sqrt[3]{P_c}$ of 2.51 and suppose that the axial-energy loss coincides with the theoretical curve of E_a/P (fig. 32). Then, 1.5 percent of the power of each propeller goes into axial-energy loss and 1.5 percent goes into rotational-energy loss. In other words, 3 percent of the total power of both propellers is lost in axial-energy and rotational-energy losses. Now, if the total power is put into counterrotating propellers of the same diameter, P_c and therefore E_a/P will be doubled so that there will be no gain in efficiency even though all the rotational-energy loss is recovered. Above an operating condition corresponding to a value of $1/\sqrt[3]{P_c}=2.51$, some gain might be expected by using counterrotating propellers similar to propeller C; below this value of $1/\sqrt[3]{P_c}$, from considerations of propeller efficiency, it is more advantageous to mount the propellers independently of each other.

The curves for the three-blade, the four-blade, and the six-blade Goldstein propellers show that counterrotating propellers become more and more attractive as the propeller solidity is increased. An estimate of the gain in propeller efficiency that can be realized by the use of counterrotating propellers may be obtained from figure 32.

Several examples are given in table I to illustrate the application of the results. For the first example, it is assumed that a 14-foot-diameter, three-blade propeller absorbs 1500 horsepower at a speed of 310 miles per hour. In the second example, it is assumed that an 11-foot-diameter, three-blade propeller absorbs 1500 horsepower at a speed of 450 miles per hour. In each example, the power losses of two propellers mounted independently of each other are compared with the losses of two propellers, one right-hand and one left-hand mounted in tandem, that absorb the same total power. It is assumed for the case of the propellers mounted independently of each other that none of the rotation is taken out of the slipstream by the wing or other airplane parts, that is, all the rotational energy is lost, and it is further assumed that the counterrotating tandem propellers recover all the rotational-energy loss. Each example includes the comparison of the power losses for each of the three types of propeller in figure 32. The losses are also given for one six-blade Goldstein propeller that absorbs the same total power.

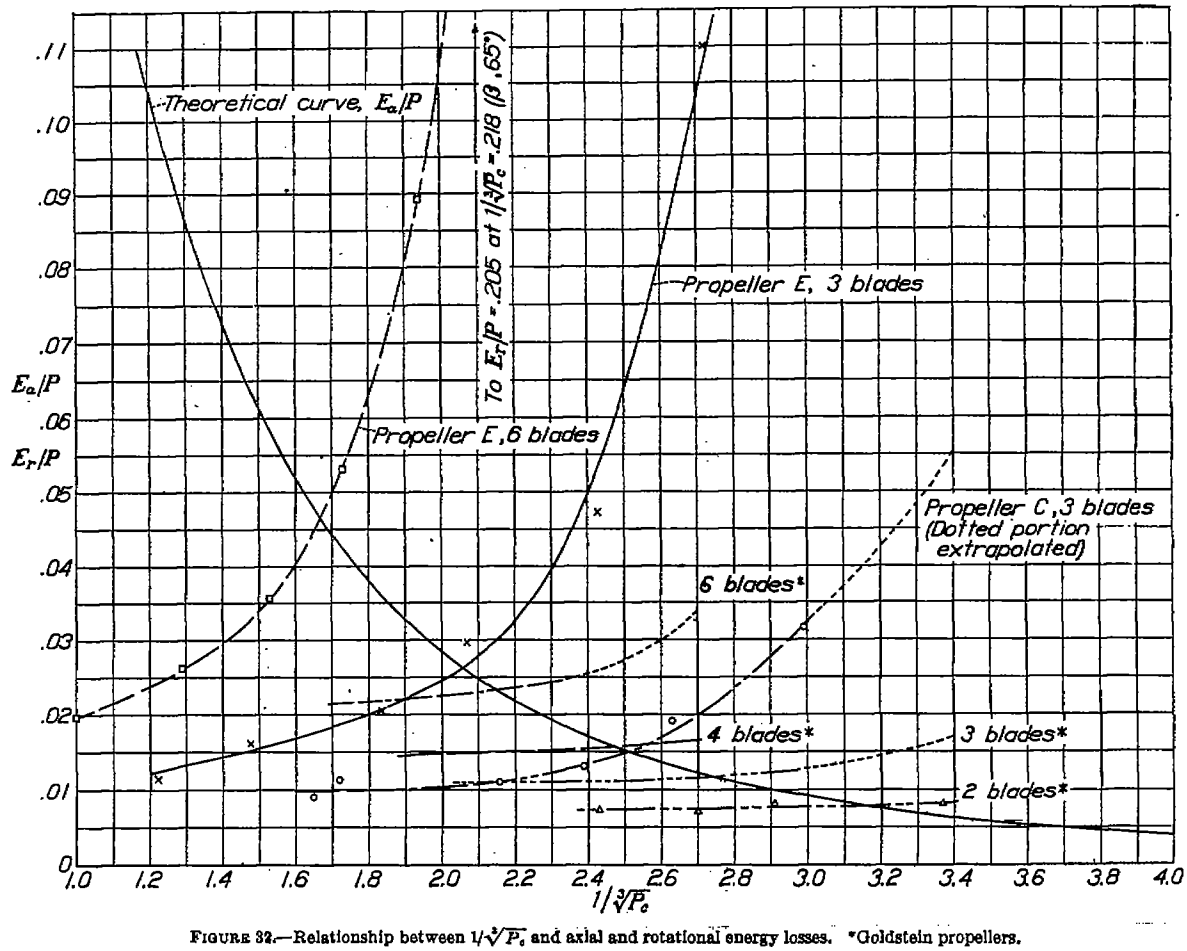

FIGURE 32.—Relationship between $1/\sqrt[3]{P_c}$ and axial and rotational energy losses. *Goldstein propellers.

TABLE 1.—APPLICATION OF RESULTS

Propeller	Number of blades	Diameter (ft)	Velocity (mph)	Power input: Of each propeller (hp)	Power input: Total (hp)	P_c	$\frac{1}{\sqrt[3]{P_c}}$	$\frac{E_a}{P}$	$\frac{E_r}{P}$	$\frac{E_a+E_r}{P}$	Gain in efficiency with counterrotating propellers: Over 2 three-blade	Gain in efficiency with counterrotating propellers: Over 1 six-blade
Example 1												
Goldstein	3	14	310	1500	3000	0.0482	2.75	0.0117	0.0118	0.0235		
Goldstein	6	14	310	3000	3000	.0964	2.18	.0225	.0235	.0460		
Goldstein [a]	6	14	310		3000	.0964	2.18	.0225	0	.0225	0.0010	0.0235
C	3	14	310	1500	3000	.0482	2.75	.0117	.0215	.0332		
C [a]	6	14	310		3000	.0964	2.18	.0225	0	.0225	.0107	
E	3	14	310	1500	3000	.0482	2.75	.0117	.1140	.1257		
E [a]	6	14	310		3000	.0964	2.18	.0225	0	.0225	.1032	
Example 2												
Goldstein	3	11	450	1500	3000	0.0255	3.40	0.0064	0.0176	0.0234		
Goldstein	6	11	450	3000	3000	.0510	2.70	.0123	.0340	.0463		
Goldstein [a]	6	11	450		3000	.0510	2.70	.0123	0	.0123	0.0111	0.0340
C	3	11	450	1500	3000	.0255	3.40	.0064	.0552	.0616		
C [a]	6	11	450		3000	.0510	2.70	.0123	0	.0123	.0493	

[a] Right-hand and left-hand three-blade tandem propellers.

The table shows that, for the flight conditions of example 1, the power losses of two three-blade propellers having ideal load distributions and operating side by side are approximately equal to the power losses of two three-blade counterrotating tandem propellers which absorb the same total power and recover all the rotational-energy losses; whereas, the power losses for one six-blade similar propeller are 2.35 percent greater than for the counterrotating propellers. The example further shows that a gain of 1.07 percent can be realized by using the counterrotating propellers instead of two propellers with the same load distribution as propeller C and that, by the use of the counterrotating propellers instead of two propellers having the same losses as propeller E, a gain of 10.32 percent efficiency can be experimentally shown. Although this large gain in efficiency is real, it results from the initially poor torque distribution of propeller E when set at high blade angles. Data for the six-blade propeller E are not included in the table, but figure 32 shows that the rotational-energy losses for this condition of flight amount to 20.5 percent.

For the higher speed range covered in the flight conditions of example 2, the gain in efficiency by using counterrotating tandem propellers instead of two propellers having ideal load distributions is of the order of 1 percent, but the gain is 3.40 percent for one six-blade propeller. A gain in efficiency of 4.93 percent is realized by using counterrotating propellers instead of using two propellers similar to propeller C. Because of the poor load distribution of propeller E, no estimate can be made of the rotational-energy losses for the flight conditions of example 2. But the trend in the curve shows that the losses are tremendous and therefore, if a similar propeller were to be used under these flight conditions, it would be necessary to use counterrotating propellers.

In the practical application of the problem, the foregoing discussion strictly applies only to pusher propellers. In the case of tractor propellers, the wing and the tail surfaces tend to take the rotation out of the slipstream and thus to recover a considerable portion of the rotational energy that is considered here as lost. This result means that counterrotating propellers in tractor positions will not become attractive from considerations of aerodynamic efficiency except at even higher speeds than the curves of figure 32 indicate. The foregoing analysis shows that, for a propeller of low solidity with optimum distribution of thrust and torque, little is to be gained by the use of counterrotating propellers even at high speeds. For propellers of poor distribution, especially propellers having a high loading over the inner sections such as propeller E, the rotational-energy losses increase so rapidly at very high speeds that a large increase in efficiency may be shown by using counterrotating propellers.

CONCLUDING REMARKS

1. A knowledge of the distribution of thrust and torque along the propeller blade permits the analysis of propeller performance. The performance of the test propeller has been analyzed, and a method of applying the analysis to other data for higher blade-angle settings has been presented.

2. The loss in efficiency due to the rotational velocity is always small for a propeller of optimum design, being only of the order of 1 percent for a low-solidity propeller. The loss of efficiency from this source may become quite large, however, at high blade-angle settings for a propeller with improper load distribution.

3. Counterrotating propellers are attractive from considerations of aerodynamic efficiency only when propellers of high solidity are used. Large gains in

propeller efficiency with counterrotating propellers may be expected only if propellers of poor torque distribution are used.

4. If high-solidity propellers are selected because of limitations on propeller diameter, it may be useful to resort to counterrotating propellers to eliminate the effect of the engine torque on the flying characteristics of the airplane. Only a small direct gain in propeller efficiency is normally to be expected.

5. The effects of body shape on the thrust and the torque distributions of the propeller are shown.

6. The average angle of twist in the propeller slipstream is shown to be a unique function of the torque coefficient Q_c and charts are given to help estimate the angle.

7. The increase in total pressure along the radius behind the propeller is given as a function of the power coefficient $1/\sqrt[3]{P_c}$. It is of use in estimating the available pressure that can be obtained for air intakes behind the propeller.

LANGLEY MEMORIAL AERONAUTICAL LABORATORY,
NATIONAL ADVISORY COMMITTEE FOR AERONAUTICS,
LANGLEY FIELD, VA., *July 19, 1940.*

REFERENCES

1. Glauert, H.: Airplane Propellers. Vol. IV, div. L of Aerodynamic Theory, W. F. Durand, ed., Julius Springer (Berlin), 1935, pp. 169–360.
2. Stickle, George W.: Measurement of the Differential and Total Thrust and Torque of Six Full-Scale Adjustable-Pitch Propellers. Rep. No. 421, NACA, 1932.
3. Weick, Fred E., and Wood, Donald H.: The Twenty-Foot Propeller Research Tunnel of the National Advisory Committee for Aeronautics. Rep. No. 300, NACA, 1928.
4. Lock, C. N. H., and Bateman, H.: Wind Tunnel Tests of High Pitch Airscrews. Part II. Variations of Blade Width and Blade Section. R. & M. No. 1729, British A. R. C., 1936.
5. Stickle, George W., Crigler, John L., and Naiman, Irven: Effect of Body Nose Shape on the Propulsive Efficiency of a Propeller. Rep. No. 725, NACA, 1941.
6. Lesley, E. P.: Tandem Air Propellers—II. T. N. (No. 822), NACA, 1941.